# Spatial profiling reveals TREM2$^{+}$ macrophages as central to *Mycobacterium tuberculosis* pathogenesis in human pulmonary tuberculosis

Rosane M. B. Teles[1], Chaouki Benabdessalem[2], Jonathan Perrie[3], Cenfu Wei[4], Julie West[1], Bruno J. de Andrade Silva[1], Priscila R. Andrade[1], Lilah A. Mansky[1], Prajan Divakar[5] Linda Fischbacher[6], Karen Lam[1], Feiyang Ma[1], Kimia Rategh[1], Aparna Pillai[1], Samuel M. French[7], Emna Romdhane[8], Mohamed-Ridha Barbouche[2*], Eynav Klechevsky[9], Marco Colonna[9], Adrie J. C. Steyn[10], Steven J. Bensinger[11, 12], Daniel L. Barber[13], Soumaya Rammeh[8], Parambir S. Dulai[4], Bryan D. Bryson[14], Matteo Pellegrini[3], John T. Belisle[6], Barry R. Bloom[15] and Robert L. Modlin[1, 11]

**Affiliations:**

[1]Division of Dermatology, Department of Medicine, [3]Department of Molecular, Cell, and Developmental Biology, [7]Department of Pathology, [11]Department of Microbiology, Immunology and Molecular Genetics, [12]Department of Molecular and Medical Pharmacology, David Geffen School of Medicine, University of California, Los Angeles, CA, USA, [2]Laboratory of Transmission, Control and Immunobiology of Infections, Institut Pasteur de Tunis, University of Tunis El Manar, Tunis, Tunisia, [4]Northwestern University, Chicago, IL, USA, [5]Bruker Spatial Biology, Bothell, WA 98021, [6]Department of Microbiology, Immunology and Pathology, Colorado State University, Fort Collins, CO, USA, [8]Department of Pathology, Charles Nicolle Hospital, Tunis, Tunisia; LR23ES02, Faculté de Médecine de Tunis, Université de Tunis El Manar, Tunis, Tunisia, [9]Department of Pathology & Immunology, Washington University in St. Louis, St. Louis, MO, USA, [10]Africa Health Research Institute, Durban, South Africa, T Lymphocyte Biology Section, [13]Laboratory of Parasitic Diseases, NIAID, NIH, Bethesda, MD, 20892, USA, [14]Massachusetts Institute of Technology, Cambridge, MA, USA, [15]Harvard T.H. Chan School of Public Health. *Current address: Department of Microbiology, Immunology and Infectious Diseases, College of Medicine and Medical Sciences, Arabian Gulf University, Manama, Bahrain

**ABSTRACT**

Tuberculosis (TB) remains a major global health challenge. While organized granulomas have long been the focus of TB pathogenesis research, the early development of TB pneumonia typically preceding granuloma formation has been underexplored. Using spatial transcriptomics, high-resolution proteomics, and scRNA-seq on human pulmonary TB lesions, we reveal a striking compartmentalization of immune responses between early pneumonia and mature granulomas. The immunologic composition of granulomas was distinct from the pneumonia; granulomas are enriched for antimicrobial gene expression in both macrophages and T cells and show reduced bacterial antigen burden. In contrast, TREM2-expressing foamy macrophages are the predominant cell type occupying alveolar spaces in TB pneumonia with T cells infrequent. These TREM2$^{+}$ macrophages exhibit a lipid-associated gene program, accumulate lipid droplets, and harbor *Mycobacterium tuberculosis* antigens and mRNA corresponding to increased bacterial viability in vitro. We further show that the *M. tube*rculosis virulence lipids, PDIM and mycolic acids, potently induce and activate TREM2 signaling in TREM2-expressing macrophages, promoting an intracellular environment permissive for bacterial growth. These findings establish TREM2$^{+}$ macrophages as an early niche for *M. tuberculosis* survival and implicate TB pneumonia as a critical stage in disease transmission. Targeting this foamy macrophage population may offer opportunities to interrupt early TB progression and transmission.

## INTRODUCTION

Tuberculosis (TB), an infectious disease caused by the bacterium *Mycobacterium tuberculosis* (*M. tuberculosis*) remains a major global health problem. The World Health Organization reports greater than 10 million new cases and more than one million deaths each year[1]. The classical clinical presentation of TB involves infection of the lung, with dynamic changes in pulmonary pathology that reflect the host's immune response. The initial pulmonary infection is contained in most cases by the host's immune response, and in some cases can persist for long periods of time. Subsequent reactivation or reinfection initially results in a pneumonia, characterized by the accumulation of foamy macrophages in alveoli[2,3]. Only after the pneumonia, organized granulomas containing predominantly macrophages and lymphocytes develop to further contain the pathogen[2,4]. From studies of Medlar, the vast majority of people infected with *M. tuberculosis* do not develop clinical disease, but many have calcified lesions, indicating that the infection was contained or cleared[5]. Reactivation of TB occurs following major alteration of the host immune response, as seen in HIV coinfection[6] and anti-TNF therapy[7].

The histologic manifestations of the pneumonia are strikingly distinct from the granulomas that can develop subsequently. The pneumonia of TB is characterized by the replacement of alveolar air spaces with lipid-laden macrophages or "foamy macrophages"[8]. This accumulation of lipid-filled macrophages impairs gas exchange within the alveoli, compromising respiratory function. In contrast, the granulomas that can subsequently develop are organized structures, displaying a characteristic architecture: a central core composed of mature macrophages (epithelioid cells), and occasionally interspersed Langhans multinucleated giant cells. This central region is encapsulated by a peripheral zone predominantly populated by lymphocytes, forming a mantle-like structure. Notably, the appearance and differentiated state of macrophages differs significantly between these two pathological entities. In the pneumonia, macrophages exhibit a foamy appearance due to their high lipid content, while in organized granulomas, macrophages differentiate into epithelioid cells with distinct morphological features, and dead macrophages form the necrotic core. This divergence in macrophage phenotypes exemplifies the compartmentalized immune spectrum present within lesions in a single lung and across patients with human pulmonary TB.

Scientists have been fascinated by the striking appearance of the organized granuloma characterized by the spatial arrangement of immune cells in concentric layers, thus prompting investigation through a variety

of approaches over the past century[9-15]. A landmark observation of the granuloma structure was the microanatomic compartmentalization of the T cell response in TB[10] and other granulomatous diseases[16,17], with $CD4^+$ T cells distributed throughout the granuloma and $CD8^+$ T cells localized to the mantle surrounding the granuloma. Subsequently, the granuloma core was described as a “pro-inflammatory environment characterized by the presence of antimicrobial peptides, reactive oxygen and nitrogen species and pro-inflammatory eicosanoids”[11].

Here, using scRNA-seq, spatial transcriptomics (GeoMx), spatial protein phenotyping (CosMx protein array), and in situ hybridization, we investigated the spatial landscape of human pulmonary TB at the site of disease, directly profiling patient lung lesions to obtain clinically relevant insights. Here we present the distinct patterns of cellular and molecular organization of the granulomas as compared to the pneumonia in biopsy specimens of the same patients including antimicrobial responses aimed at containing the pathogen. The major strategy for controlling infectious diseases is to interrupt transmission and this work indicates how the infected “foamy macrophages” in TB pneumonia potentially contribute to transmission early in the infection. Notably, this early pneumonia often develops before any overt symptoms, raising the concern that asymptomatic patients may unknowingly harbor transmissible infection.

## RESULTS

### What are the differences in gene expression profiles between TB pneumonia and organized granulomas?

We performed GeoMx spatial profiling on four biopsy specimens from patients with pulmonary TB (**Figure 1, Supplemental Table 1, Supplemental Figure 1**), selecting 59 regions of interest (ROIs) yielding a total of ~380 million aligned reads (**Supplemental Table 2**). Histologic examination of the PTB 21.1 biopsy specimen showed the presence of pneumonia, granulomas and caseous necrosis (**Figure 1A**). Individual granulomas or groups of granulomas (**Figure 1B, C**) were located adjacent or within the pneumonia. The alveoli in the pneumonia were filled with aggregates of foamy macrophages (**Figure 1D**). The granulomas were well-organized, with a core containing mature macrophages (epithelioid cells) and Langhans giant cells surrounded by a mantle zone of lymphocytes. Regions of dense lymphocytic infiltrates were also associated with the mantle zone.

Using the GeoMx Digital Spatial Profiler (Nanostring/Bruker), we selected regions of interest (ROIs) in the core and mantle of granulomas, as well as in alveoli for gene expression analysis (**Figure 1E-H**). Projection of the high-dimensional gene profiling data by uniform manifold approximation and projection (UMAP) revealed three distinct clusters corresponding to the location of ROIs from the alveoli, core, and mantle (**Figure 1I, Supplemental Figure 2**). To understand the mechanisms that contribute to host defense and/or pathogenesis, differential gene expression (DGE) analysis using DESeq2 across alveoli, core, and mantle regions was performed for pairwise comparisons between each region. In the alveoli vs. the granuloma core and mantle, we identified more robust expression of genes encoding surfactant proteins produced by alveolar epithelial type 2 cells (AET2; SFTPC, SFTPA2), TREM2$^{+}$ macrophages, such as lipid metabolism-related proteins (APOC1, APOE, LIPA) and scavenger receptors (MSR1, CD36, and CD163) (**Supplemental Figure 3A, B**). In contrast, the granuloma core in comparison to the alveoli and granuloma mantle expressed genes typical of M1-like macrophage markers (SOD2, IDO1) including antimycobacterial pathways (IL1B, IL32 and CYP27B1), CYBB, an oxidase related to antimicrobial host defense against TB[18] as well as and genes encoding a family of metallothionein proteins (MT1/2 isoforms) (**Supplemental Figure 3A, C**). When the mantle zone was compared to the granuloma core or alveoli, T cell (TRBC1, TRAC, CD3E, CD2) and B cell related genes (IGHM, IGHG3, IGHG2) were more abundant (**Supplemental Figure 3B, C**). By computing the set intersection

of genes differentially expressed in one region versus the other two, we identified signature genes for each region: alveoli=559, core=414, and mantle=803 (**Supplemental Table 3**).

**What are the cell types and their gene signatures that comprise human pulmonary TB?**

To study the cellular composition of human pulmonary TB, scRNA-sequencing was performed from the FFPE specimens from the four patients with pulmonary TB. A total of 45,023 cells were studied (detecting an average of 1017 genes and 1643.1 transcripts per cell). A total of 27 cell types were identified by comparing to the scRNA-seq cluster signatures to known cell signatures including major cell types[19,20], a human lung atlas[21], leprosy lesions[22] and using Enrichr (**Figure 1J, Supplementary Table 4, Supplemental Figure 4A**) There were seven different lymphocyte subpopulations and ten different myeloid subpopulations (**Figure 1J**). The myeloid populations contain five types of macrophages: “IFN-activated macrophages”, “SPP1$^+$ macrophages”, “interstitial macrophages”, “alveolar macrophages” and “TREM2$^+$ macrophages”. The T cell populations included: CD8$^+$ T cells, naïve (or resting) T cells, Th17 cells (with features of Th1 cells and MAITs), NK/T-CTL/GD cells, and Tregs). These populations were stable across the four different patients (**Supplementary Figure 4B**). These data provide new high-resolution characterization of cells within the human infection site.

**What are the differences in the frequency of cell types as defined by gene expression signatures between and TB pneumonia and the organized granulomas?**

We identified the location of the cell types derived from scRNA-seq data of the four human pulmonary TB samples by overlapping with the gene signatures from the GeoMx spatial analysis of the alveoli, core and mantle regions. We used the Jaccard index to quantify the agreement between scRNA-seq-derived cell type signature genes and region-specific GeoMx spatial transcriptomic signatures, enabling an unbiased comparison based on shared gene identity rather than expression levels, and thereby facilitating inference of the predominant cell types within each spatial compartment. We identified “TREM2$^+$ macrophages”, “alveolar macrophages” and “interstitial macrophages” in the alveoli (**Figure 1K**). The location of “TREM2$^+$ macrophages” in the alveoli is consistent with the location of foamy macrophages in alveoli. The granuloma core contained “SPP1$^+$ macrophages”, “IFN-activated macrophages” and “Th17 cells”. The granuloma mantle zone contained “B cells”, “plasma cells”, “CD8$^+$ T cells” and “LAMP3$^+$ DC”.

Overlap of the GeoMx spatial signature genes from each region with cell type markers from a scRNA-seq healthy lung atlas[21] revealed that the alveoli had the strongest overlap with gene signatures from “AET1” and “AET2” (**Supplemental Figure 5A**). The granuloma core showed the strongest overlap with the gene signatures from various populations of monocytes and macrophages. Both the alveoli and the core gene signatures showed strong statistical agreement with “TREM2$^+$ macrophages” (q values $<10^{-10}$). The granuloma mantle had the strongest overlap with gene signatures from “B cells” and various T cell and NK cell populations. Overlap of key gene sets with our previous studies of leprosy lesion scRNA-seq data[22] revealed that the alveoli had the strongest overlap with gene signatures from “TREM2$^+$ macrophages”, consistent with the location of foamy macrophages in alveoli (**Supplemental Figure 5B**). The granuloma core showed the strongest overlap with gene signatures from “M1-like macrophages”, “type I IFN macrophages”, “Th17 cells”, and “T-CTLs”. The mantle zone showed the strongest overlap with gene signatures from “B cells” and T cell subsets as well as “DCs”.

We further assessed the different host responses in the granuloma and pneumonia by functional pathway analysis of the pulmonary TB DGE signatures from the GeoMx spatial profiling data. The alveoli DGEs were enriched for lipid metabolism, localization and transport, typical for TREM2$^+$ macrophages, as well as surfactant metabolism (**Supplemental Figure 6A**). The core DGEs were enriched for innate immune responses including responses to bacterium while the mantle DGEs were enriched for T and B cell pathways, consistent with the histology of this region and the overlap with leprosy scRNA-seq marker sets. Similar analysis of the pulmonary TB scRNA-seq myeloid cell gene signatures indicated that IFN-activated macrophages and SPP1+ macrophages were enriched for “defense response to bacterium” and “antimicrobial humoral immune response mediated by antimicrobial peptide” (**Supplemental Figure 6B**). The TREM2$^+$ macrophage and alveolar macrophages were enriched in lipid metabolism pathways.

**What are the differences in expression of genes encoding proteins involved in antimicrobial mechanisms in the organized granulomas and the TB pneumonia?**

Given that a major function of granulomas is to contain and kill invading pathogens, we interrogated the spatial profiling gene signatures for possible antimicrobial mechanisms, using a set of 52 key antimicrobial genes derived from the Antimicrobial Peptide Database 3 (APD3)[23] and the key antimicrobial genes relevant to

mycobacterial infection[22,24] (**Supplemental Table 5**). We detected eight antimicrobial genes in the core (adj p value 6.78E-05), five in the mantle (adj p value ns) and three in the alveoli (adj p value ns) (**Supplemental Figure 7A, B, Supplemental Table 6**). The core vs. alveoli had 15 antimicrobial genes (adj p value 3.72E-07), indicating the significant upregulation of antimicrobial gene expression in the granuloma core. Of the 52 genes which encode proteins with direct antimicrobial activity, 40 were expressed in the in the T cell and myeloid subtypes form the scRNA-seq data of human pulmonary TB (**Supplemental Figure 7C, D; Figure 1L**). In the core of the granuloma, IFN-activated macrophages expressed 15 antimicrobial genes, SPP1$^+$ macrophages eight antimicrobial genes, Th17 cells seven antimicrobial genes and NK /T-CTL/GD expressed four antimicrobial genes. In the mantle, CD8$^+$ T cells expressed three antimicrobial genes, LAMP3$^+$ DC six antimicrobial genes and cells with a monocyte signature four antimicrobial genes. Some of these genes are known to have direct antimicrobial activity against *M. tuberculosis*, CAMP which encodes cathelicidin[25] was identified in SPP1$^+$ macrophages and alveolar macrophages[25], GNLY which encodes granulysin in CD8$^+$ T cells[26] and NK/T-CTL/GD[22,27] cells, IL-26 in the Th17 cells[28] and S100A12 in monocytes[29].

**What is the localization of TREM2 signature genes in the TB pneumonia and the organized granulomas?**

To further clarify the location of TREM2$^+$ macrophages in pulmonary TB, we derived a gene signature using a consensus set of 34 TREM2$^+$macrophage related scRNA-seq gene signatures from 21 publications (**Supplemental Table 7**), ranking the frequency of genes in these signatures (**Supplemental Tables 8 and 9**). Overlap with the pulmonary TB DGEs revealed that the twelve most highly ranked TREM2 macrophage signature genes had a higher overlap with alveoli than core, with the ratio of the Jaccard indices greater than 5, for genes found in ≥22 signatures (**Supplementary Figure 8A, B**). The expression of eight genes, LGMN, CTSD, TREM2, NPC2, APOE, C1QB, GRN and C1QC was greater in the alveoli vs. core, whereas C1QA expression was almost equal and CTSB was greater in the core, with MS4A6E and FTL not detected in the GeoMx data (**Supplemental Figure 8C**). We examined the TREM2$^+$ macrophage scRNA-seq signature genes, which significantly overlapped with the gene expression in the alveoli in the GeoMx data ($q<10^{-10}$). Eleven of the twelve TREM2$^+$ macrophage genes listed above were indeed present in the TREM2$^+$ macrophage scRNA-seq cluster from our scRNA-seq data (all except MS4A6E).

Given that TREM2$^+$ macrophages are characterized by expression of lipid metabolism genes[30], we mined the TREM2$^+$ macrophage scRNA-seq data, finding enrichment for genes for lipid metabolism pathway genes characteristic of lipid localization, lipid metabolism, lipid signaling, response to lipids, cholesterol transport and cholesterol efflux (**Supplemental Figure 8D, Supplemental Table 10**). Of these, TREM2, APOE, CTSD, NPC2, PLIN2, LIPA, PSAP, CD81, APOC1 and HEXB were present in 17 of the 34 TREM2$^+$ macrophage gene signatures. Together, these data demonstrate that the TREM2$^+$ macrophages expressing lipid metabolism genes are predominantly located in the alveoli of the pulmonary TB pneumonia.

**What are the differences in the frequency of cell types as defined by specific protein determinants between and TB pneumonia and the organized granulomas?**

To further delineate the differences in cell types between the granulomas and the pneumonia in pulmonary TB biopsy specimens, we performed CosMx high resolution spatial proteomic analysis. We identified well-circumscribed granulomas, containing a core of CD68$^+$ macrophages and Langhans multinucleated giant cells with a mantle zone containing CD3$^+$ T cells and CD19$^+$ B cells (**Figure 2A, B**). The ratios and aggregation of T cells and B cells in the mantle zone varied among granulomas (**Supplemental Figure 9**). Individual or small groups of granulomas were found within the pneumonitis, with individual alveoli identified by vimentin$^+$ AETs lining the air sacs and CD163$^+$ large ovoid cells, likely TREM2$^+$ macrophages filling the air sacs (**Figure 2A, C**). Three types of alveoli were visualized: alveoli containing predominantly CD163$^+$ macrophages (**Figure 2D**), alveoli containing macrophages co-expressing CD68$^+$ and CD163$^+$ (**Figure 2E**), and alveoli containing CD163$^+$ macrophages, which corresponded to the foamy macrophages visualized by H&E staining and CD3$^+$ T cells (**Figure 2F, Supplemental Figure 10**).

CD163$^+$ macrophages were observed in spatial proximity with CD3$^+$ T cells located in the mantle zone, consistent with the established understanding that granulomas originate subsequent to and within the context of the pneumonia (**Supplemental Figure 9A, 11**). Another hallmark feature of pulmonary TB, bronchiole obstruction, a mechanism associated with spread of the infection[4], was visualized with surrounding lymphocytic infiltrate containing T and B cells, necrosis, and obliteration of the bronchiolar epithelium such that the airway was occluded by necrotic granulomas (**Supplemental Figure 12**).

By standard immunohistology, we detected $CD3^+$ and $CD4^+$ lymphocytes throughout the granuloma, with $CD8^+$ and $CD20^+$ lymphocytes predominantly localized to the mantle zone (**Supplemental Figure 13A-D**). $CD68^+$ macrophages and Langhans giant cells were confirmed to be in the core of the granuloma, with CD163 identifying macrophages in alveoli (**Supplemental Figure 13E, F, and Supplemental Figure 14**).

**What are differences in colocalization of $TREM2^+$ macrophages and *M. tuberculosis* antigens in TB pneumonia and organized granulomas?**

To map the distribution of TREM2 macrophages in pulmonary TB, we performed immunohistochemistry using an anti-TREM2 monoclonal antibody, finding strong expression on the macrophages filling the alveoli, with weaker expression in granulomas and Langhans multinucleated giant cells (**Figure 3A, Supplemental Figure 15 A-D**). The macrophages within alveoli also expressed CD163, which colocalized with TREM2 (**Figure 3A, B).** The macrophages in the alveoli expressed the lipid droplet marker PLIN2, CD68, APOE, LIPA and SPP1 (**Figure 3A, Supplemental Figure 15E**). PLIN2 staining exhibited the distinct morphologic punctate morphology consistent with lipid droplets (**Supplemental Figure 16A**).

A key question remained as to where the strongest evidence for *M. tuberculosis* infection could be found, given the infrequent visualization of acid-fast bacilli in the lesions. Immunodetection of *M. tuberculosis* lipoarabinomannan (LAM) and *M. tuberculosis* purified protein derivative (PPD) protein expression showed a robust antigen signal in the alveoli compared with the granuloma (**Figure 3A, C, D, and Supplemental Figure 16 B, C**). By immunofluorescence, TREM2 colocalized with LAM in the macrophages in the pneumonia (**Figure 3C**). PLIN2 co-localized with TREM2 and LAM (**Supplemental Figure 16 D**). Recently, the Steyn lab demonstrated *M. tuberculosis* mRNA in human TB lesions, appearing as clumps or puncta, in macrophages in specimens in which acid-fast bacilli are not detected[31]. Using RNA scope with a cocktail of probes detecting *M. tuberculosis* mRNAs encoding six distinct proteins, we detected specific mRNAs as clumps in macrophages in alveoli, but as smaller puncta in macrophages in the pneumonia and granulomas (**Figure 3D, Supplemental Figure 14**). Taken together, these data indicate that $TREM2^+$ macrophages containing *M. tuberculosis* antigens correspond to the foamy lipid-loaded macrophages that accumulate in alveoli in pulmonary TB.

**What is the role of $TREM2^+$ macrophages in TB pathogenesis?**

Having demonstrated that TREM2$^+$ macrophages containing *M. tuberculosis* antigens fill the alveoli in the TB pneumonia, we next sought to determine how the interaction between the bacterium and the TREM2$^+$ macrophage contributes to disease pathogenesis. TREM2 expression is upregulated on MDMs in vitro following treatment with mammalian cytokines such as IL-4[32,33]. We determined that mycolic acids and phthiocerol dimycocerosates (PDIM) were also potent inducers of TREM2 expression in vitro, inducing approximately 50% and 55% TREM2$^+$ macrophages, respectively **(Figure 4A and Supplemental Figure 18A)**. By comparison, live *M. tuberculosis* (MOI 5 or10) led to ~30% TREM2$^+$ cells, and neither LAM nor peptidoglycan induced significant TREM2 expression.

TREM2 is a receptor protein that can be activated by a wide array of ligands, including bacterial products, DNA, lipoproteins, and phospholipids[34], including *M. tuberculosis* mycolic acids[35,36]. To measure TREM2 activation directly, we employed a chimeric reporter comprising TREM2 fused to DAP12, which clusters and fluoresces upon ITAM phosphorylation downstream of TREM2 activation [36]. Using this reporter, we determined that mycolic acids and PDIM were the strongest activators of TREM2 signaling, with TREM2 expression and activation strongly correlated ($r = 0.93$, $p = 0.007$) (**Figure 4A and Supplemental Figure 17B)**.

**Do the host and microbial signals that induce and activate TREM2$^+$ macrophages also promote lipid droplet formation?**

Infection of macrophages with *M. tuberculosis* triggers lipid droplet formation[37] a process driven by host immunometabolic reprogramming[38]. We found that treating human MDMs with either of the key *M. tuberculosis* virulence lipids, mycolic acids or PDIM, as well as with IL-4, resulted in a two-fold increase in lipid droplet accumulation compared to untreated controls (**Figure 4B, Supplemental Figure 18A**). Notably, *M. tuberculosis* infection of TREM2$^+$ macrophages led to ~50% greater lipid droplet formation relative to uninfected TREM2$^+$ controls (**Figure 4C, D**). While free mycolic acids were previously shown to induce lipid droplets[37], our data demonstrate that PDIM, a known virulence determinant[39-43] also promotes this hallmark feature of foamy macrophages.

**Do TREM2$^+$ macrophages support *M. tuberculosis* growth?**

Given the enhanced lipid droplet accumulation in TREM2$^+$ macrophages during *M. tuberculosis* infection, and the ability of virulence lipids such as mycolic acids and PDIM to induce this phenotype, we hypothesized that TREM2-driven lipid storage might create a metabolically permissive niche for bacterial survival. To test this, we infected IL-4-polarized TREM2$^+$ macrophages on day 5 with an *M. tuberculosis* H37Rv viability reporter strain[44,45] at a multiplicity of infection (MOI) of 5 for 24 hours and quantified mCherry and GFP signals by confocal microscopy. We observed that TREM2$^+$ macrophages harbored approximately twice as many viable bacteria as conventional MDMs (**Figure 4E, F**, **Supplemental Figure 18B**). This correlation between lipid accumulation and bacterial viability suggests that TREM2$^+$ macrophages establish an environment conducive to *M. tuberculosis* survival.

We next investigated whether 1,25-dihydroxyvitamin $D_3$ (1,25$(OH)_2D_3$) modulates TREM2 expression and antimicrobial function. Flow cytometric analysis revealed that 1,25$(OH)_2D_3$ decreased TREM2 expression on macrophages (**Supplemental Figure 19A, B**). To determine whether reduced TREM2 expression is related to antibacterial responses, we pre-treated macrophages with 1,25$(OH)_2D_3$. Subsequently, we infected them with a dual-fluorescent *M. tuberculosis* reporter strain (GFP-mCherry) at a multiplicity of infection (MOI) of 5. Bacterial viability was assessed by GFP signal, and confocal microscopy revealed a significant reduction in viable *M. tuberculosis* in both 1,25$(OH)_2D_3$-treated TREM2$^+$ macrophages and MDMs (**Figure 4G**). Correspondingly, colony-forming unit (CFU) assays demonstrated that both bulk MDMs and flow-sorted TREM2$^+$ macrophages treated with 1,25$(OH)_2D_3$ had markedly lower bacterial burdens after four days of infection ($p < 0.0001$), consistent with enhanced killing of intracellular bacilli (**Figure 4H**). These results suggest that vitamin D can enhance macrophage antimicrobial activity by inhibiting TREM2 expression and/or via TREM2-independent mechanisms, possibly through activation of the vitamin D response pathway[25] .

Together, these findings identify TREM2$^+$ macrophages in the alveolar space during TB pneumonia as foamy macrophages that serve as early reservoirs for *M. tuberculosis*. We propose that TREM2$^+$ macrophages represent a critical niche for intracellular persistence during the initial stages of infection.

## DISCUSSION

Since the initial description of granulomas in pulmonary TB in the 17th century[46], their characteristic spherical or cylindrical architecture composed of macrophage-rich cores surrounded by lymphocyte mantles, has been the primary focus of TB pathogenesis research[14]. Although it was recognized in the 19th century that a pneumonia typically precedes granuloma formation in pulmonary TB[47], this observation was confirmed by mid-20th century pathology studies[2,48,49]. Only in the 21st century has scientific interest shifted toward understanding the early host response during TB progression[3,50]. Traditional TB control strategies rely on patients becoming symptomatic, seeking care, receiving a diagnosis, and initiating effective therapy. Recent studies have established that asymptomatic individuals, often healthy contacts of patients, harbor viable tubercle bacteria and likely contribute to transmission[51] and that normal tidal respiration in TB patients transmits significantly more tubercle bacilli into the environment over 24h than active coughing of bacilli[52]. Hence, our focus has been on the early development of lesions in TB pneumonia, potentially contributing to asymptomatic transmission before the formation of organized granulomas and the onset of overt tissue damage.

Using spatial profiling techniques on human pulmonary TB biopsy specimens, we uncovered a striking compartmentalization of the immune responses in the early pneumonia versus the later granulomas. A major advance in our study is the identification of TREM2-expressing “lipid-associated macrophages” as the foamy macrophages filling alveoli in the TB pneumonia. These cells expressed genes and proteins involved in lipid metabolism, harbored perilipin-2-positive lipid droplets characteristic of foamy macrophages[53,54], and contained *M. tuberculosis* antigens including LAM and proteins as well as *M. tuberculosis* mRNA. In vitro, these TREM2$^+$ macrophages showed enhanced lipid droplet formation and greater *M. tuberculosis* viability relative to conventional MDMs.

Our findings establish a key link between TREM2$^+$ macrophages, lipid metabolism, and foam cell formation in the pathogenesis of tuberculosis. This macrophage phenotype is shared across multiple chronic inflammatory diseases, including atherosclerosis[55,56], Alzheimer’s disease[57,58], obesity[30], and leprosy[59]. Prior studies have shown that foamy macrophages allow *M. tuberculosis* replication during the initial stages of infection[37]. Consistent with this, we observe increased bacterial viability in TREM2$^+$ macrophages, implicating this subset in the establishment of a permissive intracellular niche. Mechanistically, TREM2 signaling has been

linked to IL-10 production and M2-like polarization, both of which can suppress antimicrobial responses. Furthermore, in pulmonary TB lesions, TREM2 expression correlated with IL-10, an immunosuppressive cytokine typically produced by M2-polarized macrophages[60]. While one report suggested that an anti-TREM2 antibody treatment reduced *M. tuberculosis* viability in human macrophages, the absence of key experimental controls, including isotype-matched antibodies and defined TREM2$^+$ cell frequencies, limits mechanistic interpretation of the result[36]. Thus, TREM2$^+$ macrophages remain an intriguing but unproven therapeutic target, and further in vivo studies are needed to evaluate potential interventions. Collectively, these findings suggest that *M. tuberculosis* exploits TREM2$^+$ macrophages to establish an intracellular niche shielded from immune clearance.

Another key insight is that the *M. tuberculosis* virulence lipid PDIM potently induces TREM2 expression and activation, matching or surpassing the effects of mycolic acids[35] and more potent than live *M. tuberculosis*[36]. PDIM is known to be essential for *M. tuberculosis* survival and virulence, contributing to phagosomal membrane damage that allows bacteria to escape into the cytosol[39-43]. In infected macrophages, PDIM is more readily released than mycolic acids, as it is non-covalently associated with the mycomembrane, whereas, mycolic acids are typically covalently linked to the arabinogalactan-peptidoglycan complex of the cell wall structure[43,61], or esterified to glycerol, glucose or trehalose. Furthermore, only free mycolic acids acted as a TREM2 ligand[35]. Thus, PDIM's loose association with the bacterial membrane and its ability to transfer to host cells[62], make it an excellent candidate as an early immune-modulating signal. PDIM also undermines host defense by inhibiting LC3-associated phagocytosis (LAP), preventing recruitment of NADPH oxidase to the phagosome[63], masking pathogen-associated molecular patterns[64], and skewing cytokine responses toward reduced pro-inflammatory and increased anti-inflammatory profiles [65,66]. Thus, we propose that PDIM is a key immunoevasive factor that simultaneously disables host antimicrobial mechanisms and reprograms macrophages towards a TREM2$^+$ macrophage state that favors bacterial survival. A recent study of *M. tuberculosis* clinical isolates revealed an increase in the relative levels of PDIM that correlated with drug resistance. The pre-XDR clinical isolate with the highest PDIM-to-phosphatidylinositol mannosides (PIM) ratio also exhibited enhanced intracellular growth compared to H37Rv[67]. These observations warrant further investigation into whether elevated PDIM production drives TREM2 activation and increased intracellular survival in drug-resistant strains.

TB pneumonia is composed of foamy macrophages[68], which accumulate cholesteryl esters and triglycerides[69], progressively filling alveolar spaces and contributing to bronchiole obstruction[70]. Following the onset of pneumonia, organized granulomas begin to form within affected regions of the lung. Our transcriptomic, spatial profiling and proteomic data reveal that TREM2$^+$ macrophages are the predominant cell type filling alveoli in this early pneumonia. These macrophages co-express lipid metabolism genes (APOE, LIPA), scavenger receptors (CD163)[60], and lipid droplet-associated proteins (PLIN2), consistent with a lipid-associated or foamy phenotype. They also harbor *M. tuberculosis* antigens and mRNAs, reinforcing their role as a permissive intracellular niche. These findings align with prior postmortem studies showing viable *M. tuberculosis* in lipid-filled macrophages[70], but we extend them by defining these cells as TREM2$^+$ and placing them in spatial context within the lung. Importantly, expression of TREM2 and CD163 was stronger in the pneumonia than in the organized granulomas, consistent with a more permissive macrophage environment in the early lesion.

The granuloma mantle zone and core represent distinct immune microenvironments, with CD4$^+$ T cells predominating in the core and CD8$^+$ T cells in the mantle[71]. Distinct populations of T cells and macrophages have been mapped to granulomas using scRNA-seq of TB lesions from zebrafish[72], mouse[73] and macaque[73,74] models of TB. Further insight into the architecture of TB granulomas has come from spatial mapping studies of multiple gene transcripts[12,75,76] or proteins[11,15,77]. For example, IDO1 protein was localized to the macrophage core of the granulomas in humans [15]. The T cell repertoire in granulomas is rich, including Th17 cells, CD8$^+$ cytotoxic T lymphocytes, and other T cell subsets that collectively express numerous antimicrobial genes. This antimicrobial gene enrichment stands in stark contrast to the pneumonia in which the TREM2$^+$ macrophages dominate alveolar spaces with T cells only sparsely distributed in a few alveoli, and the antimicrobial gene program is relatively weaker despite abundant *M. tuberculosis* antigens. These differences likely represent different stages of the immune response, with granulomas serving as sites of immune containment, with the pneumonia enabling bacterial persistence and primes for transmission. Spatially, TREM2$^+$ macrophages are also strategically located at the air-lung interface, where alveolar membrane damage[78] can contribute to a cough that can facilitate bacillary spread.

Asymptomatic (subclinical) TB has emerged as a major driver of the epidemic and a critical public health concern. Prevalence surveys indicate that roughly half of all bacteriologically confirmed pulmonary TB

cases show no overt symptoms at the time of detection[51]. Despite their lack of symptoms, these individuals are far from benign carriers: recent analyses suggest that subclinical cases may account for up to two-thirds of ongoing *M. tuberculosis* transmission globally[51]. Our findings raise the possibility that such individuals harbor TREM2$^+$ macrophages in their alveoli, silently sustaining and potentially transmitting *M. tuberculosis* in the absence of clinical symptoms[51,52]. This reinforces the importance of active case-finding and contact tracing, and supports targeting treatment to asymptomatic individuals with early lesions to interrupt transmission[79].

In summary, our findings distinguish the TB pneumonia as a critical early stage in pathogenesis of the disease from the later organization of the TB granuloma and implicate TREM2$^+$ macrophages as an early niche for *M. tuberculosis* survival and possible role in disease transmission. More broadly, the presence of TREM2$^+$ macrophages across diseases from TB and leprosy to Alzheimer's and atherosclerosis points to a general conserved immunometabolic program. Understanding how to redirect TREM2$^+$ macrophage metabolism toward protective functions could inform new therapeutic approaches not only for TB but for other chronic diseases marked by macrophage dysfunction.

**Authors contribution**

R.L.M. supervised and conceptualized the study. R.M.B.T. led the experimental work, including functional assays and CosMx, and contributed to conceptualization. C.B. contributed to sample collection, conceptualization and writing. J.P. analyzed GeoMX data and contributed to bioinformatics. C.W. analyzed FFPE RNA-seq data. J.W. contributed to CosMx, scRNA-seq, and functional analysis. B.J.A.S. performed M. tuberculosis infections and CFU assays. P.R.A. conducted RNAscope analysis. L.M., K.L., and F.M. performed bioinformatics and gene signature analyses. P.D. supported CosMx assays. L.F. contributed to mycobacterial ligand assays. K.M. and A.P. performed immunohistochemistry. S.M.F., M.R.B., E.R., and S.R. provided pathology support. A.J.C.S. supported RNAscope assays. E.K., M.C., S.B., and D.L.B. supported gene signature analyses. P.S.B., B.D.B., M.P., and J.T.B. contributed to data interpretation and manuscript revision. B.R.B. contributed to conceptualization, data interpretation and writing. The manuscript was written by R.M.B.T., B.R.B. and R.L.M.

**Acknowledgments**

The funding sources for this work were: NIH grants R01 AI022553, R01 AR040312, R01 AI166313, R01 AI169526, P50 AR080594, U01DK134321, R01DK135620 and U19AI181102.

We thank Dr. Robert Hunter for providing insight and advice on the lung pathology of tuberculosis (TB) as well as the pathogenesis of TB infection. We are grateful to Christopher C. Tai K. for assistance with single-cell RNA sequencing (scRNA-seq) from FFPE pulmonary TB samples, and to Annaliza Legaspi for help with blood donor selection and processing. We acknowledge the University of California–Los Angeles California NanoSystems Institute Advanced Light Microscopy Core Facility for assistance with confocal studies (RRID: SCR_022789). We thank Barbara Dillon from the UCLA High Containment Facilities for support with BSL-3–required assays. We also thank the UCLA Technology Center for Genomics & Bioinformatics (TCGB) for assistance with GeoMX and scRNA-seq, the Translational Pathology Core Laboratory (TPCL) for sectioning FFPE TB samples for CosMx and scRNA-seq, and the UCLA Jonsson Comprehensive Cancer Center (JCCC) Flow Cytometry Core Facility for support with flow cytometry assays.

References


1. WHO. *Global tuberculosis report 2024*, (World Health Organization, Geneva, 2024).
2. Cannetti, G. The tubercle bacillus. (Springer Publishing Company, Inc., New York (NY), 1955).
3. Hunter, R.L. Pathology of post primary tuberculosis of the lung: an illustrated critical review. *Tuberculosis (Edinburgh, Scotland)* **91**, 497-509 (2011).
4. Hunter, R.L. Tuberculosis as a three-act play: A new paradigm for the pathogenesis of pulmonary tuberculosis. *Tuberculosis (Edinburgh, Scotland)* **97**, 8-17 (2016).
5. Medlar, E.M. The behavior of pulmonary tuberculous lesions; a pathological study. *Am Rev Tuberc* **71**, 1-244 (1955).
6. Pitchenik, A.E.*, et al.* Opportunistic infections and Kaposi's sarcoma among Haitians: evidence of a new acquired immunodeficiency state. *Ann. Intern. Med.* **98**, 277-284 (1983).
7. Keane, J.*, et al.* Tuberculosis associated with infliximab, a tumor necrosis factor alpha-neutralizing agent. *N. Engl. J. Med.* **345**, 1098-1104 (2001).
8. Russell, D.G., Cardona, P.J., Kim, M.J., Allain, S. & Altare, F. Foamy macrophages and the progression of the human tuberculosis granuloma. *Nat Immunol* **10**, 943-948 (2009).
9. Dannenberg, A.M., Jr., Ando, M. & Shima, K. Macrophage accumulation, division, maturation, and digestive and microbicidal capacities in tuberculous lesions. 3. The turnover of macrophages and its relation to their activation and antimicrobial immunity in primary BCG lesions and those of reinfection. *J. Immunol.* **109**, 1109-1121 (1972).
10. Shen, J.Y., Barnes, P.F., Rea, T.H. & Meyer, P.R. Immunohistology of tuberculous adenitis in symptomatic HIV infection. *Clin. Exp. Immunol.* **72**, 186-189 (1988).
11. Marakalala, M.J.*, et al.* Inflammatory signaling in human tuberculosis granulomas is spatially organized. *Nat. Med.* **22**, 531-538 (2016).
12. Carow, B.*, et al.* Spatial and temporal localization of immune transcripts defines hallmarks and diversity in the tuberculosis granuloma. *Nature communications* **10**, 1823 (2019).
13. Ji, A.L.*, et al.* Multimodal Analysis of Composition and Spatial Architecture in Human Squamous Cell Carcinoma. *Cell* **182**, 497-514.e422 (2020).
14. Wells, G.*, et al.* Micro-Computed Tomography Analysis of the Human Tuberculous Lung Reveals Remarkable Heterogeneity in Three-dimensional Granuloma Morphology. *Am. J. Respir. Crit. Care Med.* **204**, 583-595 (2021).
15. McCaffrey, E.F.*, et al.* The immunoregulatory landscape of human tuberculosis granulomas. *Nat. Immunol.* **23**, 318-329 (2022).
16. Modlin, R.L., Hofman, F.M., Taylor, C.R. & Rea, T.H. T lymphocyte subsets in the skin lesions of patients with leprosy. *J. Am. Acad. Dermatol.* **8**, 182-189 (1983).
17. Modlin, R.L.*, et al.* In situ demonstration of T lymphocyte subsets in granulomatous inflammation: leprosy, rhinoscleroma and sarcoidosis. *Clin. Exp. Immunol.* **51**, 430-438 (1983).
18. Bustamante, J.*, et al.* Germline CYBB mutations that selectively affect macrophages in kindreds with X-linked predisposition to tuberculous mycobacterial disease. *Nat Immunol* **12**, 213-221 (2011).
19. Inkeles, M.S.*, et al.* Comparison of molecular signatures from multiple skin diseases identifies mechanisms of immunopathogenesis. *J. Invest. Dermatol.* **135**, 151-159 (2015).
20. Inkeles, M.S.*, et al.* Cell-type deconvolution with immune pathways identifies gene networks of host defense and immunopathology in leprosy. *JCI insight* **1**, e88843 (2016).
21. Travaglini, K.J.*, et al.* A molecular cell atlas of the human lung from single-cell RNA sequencing. *Nature* **587**, 619-625 (2020).
22. Ma, F.*, et al.* The cellular architecture of the antimicrobial response network in human leprosy granulomas. *Nat. Immunol.* **22**, 839-850 (2021).
23. Wang, G., Li, X. & Wang, Z. APD3: the antimicrobial peptide database as a tool for research and education. *Nucleic Acids Res.* **44**, D1087-1093 (2016).
24. Andrade, P.R.*, et al.* Dynamics of Th1/Th17 responses and antimicrobial pathways in leprosy skin lesions. *J. Clin. Invest.* (2025).
25. Liu, P.T.*, et al.* Toll-like receptor triggering of a vitamin D-mediated human antimicrobial response. *Science* **311**, 1770-1773 (2006).
26. Stenger, S.*, et al.* An antimicrobial activity of cytolytic T cells mediated by granulysin. *Science* **282**, 121-125 (1998).

27. Balin, S.J., *et al.* Human antimicrobial cytotoxic T lymphocytes, defined by NK receptors and antimicrobial proteins, kill intracellular bacteria. *Sci Immunol* **3**, 10.1126/sciimmunol.aat7668 (2018).
28. Dang, A.T., *et al.* IL-26 contributes to host defense against intracellular bacteria. *J. Clin. Invest.* **129**, 1926-1939 (2019).
29. Realegeno, S., *et al.* S100A12 Is Part of the Antimicrobial Network against Mycobacterium leprae in Human Macrophages. *PLoS Pathog.* **12**, e1005705 (2016).
30. Jaitin, D.A., *et al.* Lipid-Associated Macrophages Control Metabolic Homeostasis in a Trem2-Dependent Manner. *Cell* **178**, 686-698 e614 (2019).
31. Nargan, K., *et al.* Spatial distribution of Mycobacterium tuberculosis mRNA and secreted antigens in acid-fast negative human antemortem and resected tissue. *EBioMedicine* **105**, 105196 (2024).
32. Turnbull, I.R., *et al.* Cutting edge: TREM-2 attenuates macrophage activation. *J. Immunol.* **177**, 3520-3524 (2006).
33. Do, T.H., *et al.* TREM2 macrophages induced by human lipids drive inflammation in acne lesions. *Sci Immunol* **7**, eabo2787 (2022).
34. Kober, D.L. & Brett, T.J. TREM2-Ligand Interactions in Health and Disease. *J. Mol. Biol.* **429**, 1607-1629 (2017).
35. Iizasa, E., *et al.* TREM2 is a receptor for non-glycosylated mycolic acids of mycobacteria that limits anti-mycobacterial macrophage activation. *Nature communications* **12**, 2299 (2021).
36. Dabla, A., *et al.* TREM2 Promotes Immune Evasion by Mycobacterium tuberculosis in Human Macrophages. *mBio* **13**, e0145622 (2022).
37. Peyron, P., *et al.* Foamy macrophages from tuberculous patients' granulomas constitute a nutrient-rich reservoir for M. tuberculosis persistence. *PLoS Pathog.* **4**, e1000204 (2008).
38. Knight, M., Braverman, J., Asfaha, K., Gronert, K. & Stanley, S. Lipid droplet formation in Mycobacterium tuberculosis infected macrophages requires IFN-gamma/HIF-1alpha signaling and supports host defense. *PLoS Pathog.* **14**, e1006874 (2018).
39. McDonough, K.A., Kress, Y. & Bloom, B.R. Pathogenesis of tuberculosis: Interaction of Mycobacterium tuberculosis with macrophages. *Infect Immun* **61**, 2763-2773 (1993).
40. Teitelbaum, R., *et al.* Mycobacterial infection of macrophages results in membrane-permeable phagosomes. *Proc. Natl. Acad. Sci. U. S. A.* **96**, 15190-15195 (1999).
41. van der, W.N., *et al.* M. tuberculosis and M. leprae translocate from the phagolysosome to the cytosol in myeloid cells. *Cell* **129**, 1287-1298 (2007).
42. Quigley, J., *et al.* The Cell Wall Lipid PDIM Contributes to Phagosomal Escape and Host Cell Exit of Mycobacterium tuberculosis. *mBio* **8**(2017).
43. Mulholland, C.V., *et al.* Propionate prevents loss of the PDIM virulence lipid in Mycobacterium tuberculosis. *Nature microbiology* **9**, 1607-1618 (2024).
44. Martin, C.J., *et al.* Efferocytosis is an innate antibacterial mechanism. *Cell Host Microbe* **12**, 289-300 (2012).
45. Ouimet, M., *et al.* Mycobacterium tuberculosis induces the miR-33 locus to reprogram autophagy and host lipid metabolism. *Nat. Immunol.* **17**, 677-686 (2016).
46. de Le Boe Sylvius, F. *Francisci Deleboe, Sylvii Opera medica*, (Apud D. Elsevirium et A. Wolfgang, 1679).
47. Laennec, R.T.H. A treatise on the diseases of the chest: in which they are described according to their anatomical characters, and their diagnosis established on a new principle by means of acoustick instruments. *(No Title)* (1821).
48. Rich, A.R. *The pathogenesis of tuberculosis*, (CC Thomas, 1944).
49. Levine, E.R. Classification of reinfection pulmonary tuberculosis. *The Fundamentals of Pulmonary Tuberculosis and its Complications for Students, Teachers and Practicing Physicians (Hayes E, Ed), Thomas, Springfield*, 97-113 (1949).
50. Hunter, R.L., Actor, J.K., Hwang, S.A., Karev, V. & Jagannath, C. Pathogenesis of post primary tuberculosis: immunity and hypersensitivity in the development of cavities. *Ann. Clin. Lab. Sci.* **44**, 365-387 (2014).
51. Emery, J.C., *et al.* Estimating the contribution of subclinical tuberculosis disease to transmission: An individual patient data analysis from prevalence surveys. *eLife* **12**(2023).
52. Dinkele, R., *et al.* Aerosolization of Mycobacterium tuberculosis by Tidal Breathing. *Am. J. Respir. Crit. Care Med.* **206**, 206-216 (2022).

53. Nuotio, K., *et al.* Adipophilin expression is increased in symptomatic carotid atherosclerosis: correlation with red blood cells and cholesterol crystals. *Stroke* **38**, 1791-1798 (2007).
54. Dib, L., *et al.* Lipid-associated macrophages transition to an inflammatory state in human atherosclerosis increasing the risk of cerebrovascular complications. *Nature cardiovascular research* **2**, 656-672 (2023).
55. Cochain, C., *et al.* Single-Cell RNA-Seq Reveals the Transcriptional Landscape and Heterogeneity of Aortic Macrophages in Murine Atherosclerosis. *Circ. Res.* **122**, 1661-1674 (2018).
56. Patterson, M.T., *et al.* Trem2 promotes foamy macrophage lipid uptake and survival in atherosclerosis. *Nature cardiovascular research* **2**, 1015-1031 (2023).
57. Ruiz, A., *et al.* Assessing the role of the TREM2 p. R47H variant as a risk factor for Alzheimer's disease and frontotemporal dementia. *Neurobiol. Aging* **35**, 444. e441-444. e444 (2014).
58. Krasemann, S., *et al.* The TREM2-APOE Pathway Drives the Transcriptional Phenotype of Dysfunctional Microglia in Neurodegenerative Diseases. *Immunity* **47**, 566-581 e569 (2017).
59. Ma, F., *et al.* Single cell and spatial sequencing define processes by which keratinocytes and fibroblasts amplify inflammatory responses in psoriasis. *Nature communications* **14**, 3455 (2023).
60. Shang, X., *et al.* Triggering Receptor Expressed on Myeloid Cells 2 Mediates the Involvement of M2-Type Macrophages in Pulmonary Tuberculosis Infection. *Journal of inflammation research* **17**, 1919-1928 (2024).
61. Ramon-Luing, L.A., Palacios, Y., Ruiz, A., Tellez-Navarrete, N.A. & Chavez-Galan, L. Virulence Factors of Mycobacterium tuberculosis as Modulators of Cell Death Mechanisms. *Pathogens* **12**(2023).
62. Augenstreich, J., *et al.* Phthiocerol Dimycocerosates From Mycobacterium tuberculosis Increase the Membrane Activity of Bacterial Effectors and Host Receptors. *Frontiers in cellular and infection microbiology* **10**, 420 (2020).
63. Mittal, E., *et al.* Mycobacterium tuberculosis virulence lipid PDIM inhibits autophagy in mice. *Nature microbiology* **9**, 2970-2984 (2024).
64. Cambier, C.J., *et al.* Mycobacteria manipulate macrophage recruitment through coordinated use of membrane lipids. *Nature* **505**, 218-222 (2014).
65. Hamerman, J.A., *et al.* Cutting edge: inhibition of TLR and FcR responses in macrophages by triggering receptor expressed on myeloid cells (TREM)-2 and DAP12. *J. Immunol.* **177**, 2051-2055 (2006).
66. Zhai, Q., *et al.* Triggering Receptor Expressed on Myeloid Cells 2, a Novel Regulator of Immunocyte Phenotypes, Confers Neuroprotection by Relieving Neuroinflammation. *Anesthesiology* **127**, 98-110 (2017).
67. Schami, A., *et al.* Drug resistant Mycobacterium tuberculosis strains have altered cell envelope hydrophobicity that influences infection outcomes in human macrophages. *Sci. Rep.* **14**, 30840 (2024).
68. Canetti, G. *The Tubercle Bacillus in the Pulmonary Lesion of Man: Histobacteriology and Its Bearing on the Therapy of Pulmonary Tuberculosis*, (Springer Publishing Company, 1955).
69. Bedard, M., *et al.* A terpene nucleoside from M. tuberculosis induces lysosomal lipid storage in foamy macrophages. *J. Clin. Invest.* **133**(2023).
70. Hunter, R.L., Jagannath, C. & Actor, J.K. Pathology of postprimary tuberculosis in humans and mice: contradiction of long-held beliefs. *Tuberculosis (Edinb )* **87**, 267-278 (2007).
71. Barnes, P.F., *et al.* Compartmentalization of a CD4+ T lymphocyte subpopulation in tuberculous pleuritis. *J. Immunol.* **142**, 1114-1119 (1989).
72. Cronan, M.R., *et al.* A non-canonical type 2 immune response coordinates tuberculous granuloma formation and epithelialization. *Cell* **184**, 1757-1774 e1714 (2021).
73. Esaulova, E., *et al.* The immune landscape in tuberculosis reveals populations linked to disease and latency. *Cell Host Microbe* **29**, 165-178 e168 (2021).
74. Gideon, H.P., *et al.* Multimodal profiling of lung granulomas in macaques reveals cellular correlates of tuberculosis control. *Immunity* **55**, 827-846 e810 (2022).
75. Magoulopoulou, A., *et al.* Spatial Resolution of Mycobacterium tuberculosis Bacteria and Their Surrounding Immune Environments Based on Selected Key Transcripts in Mouse Lungs. *Front. Immunol.* **13**, 876321 (2022).
76. Sawyer, A.J., *et al.* Spatial mapping reveals granuloma diversity and histopathological superstructure in human tuberculosis. *J. Exp. Med.* **220**(2023).
77. Qiu, X., *et al.* Spatial transcriptomic sequencing reveals immune microenvironment features of Mycobacterium tuberculosis granulomas in lung and omentum. *Theranostics* **14**, 6185-6201 (2024).
78. Belton, M., *et al.* Hypoxia and tissue destruction in pulmonary TB. *Thorax* **71**, 1145-1153 (2016).

79. Bloom, B.R. A half-century of research on tuberculosis: Successes and challenges. *J. Exp. Med.* **220**(2023).

# Figure 1

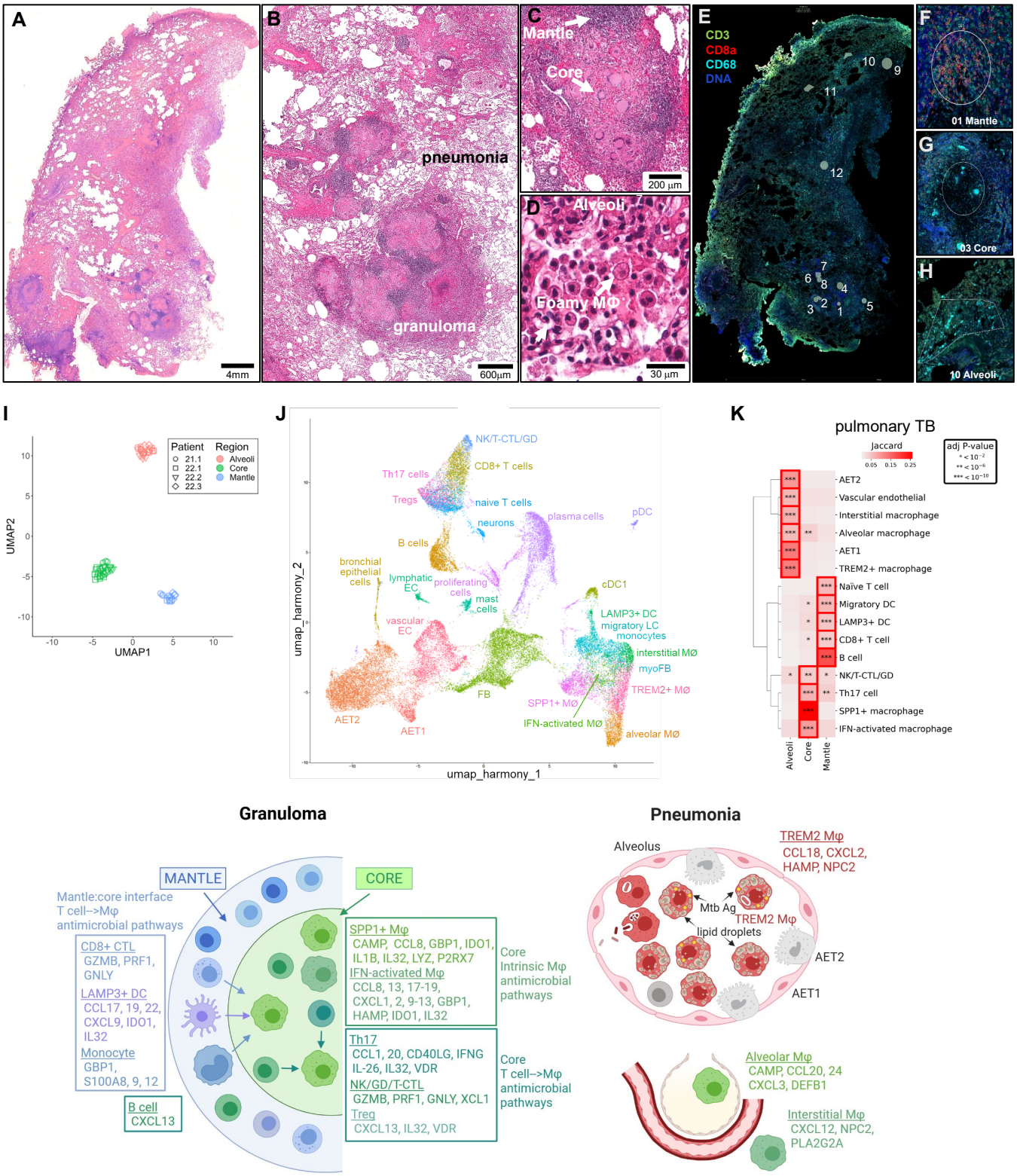


**Figure 1**. GeoMx spatial profiling of the human transcriptome in pulmonary TB (PTB). (A-B) Pulmonary TB biopsy specimen from PTB 21.1a, H&E. (C) Organized granuloma, H&E, (D) Pneumonitis showing alveoli with foamy macrophages, (E) Regions of interest (ROI), serial section, immunofluorescence, (F) Mantle- ROI 01, (G) Core- ROI 03, (H) Alveoli- ROI 10, (I) UMAP representation of all ROIs. (J) UMAP representation of PTB cell signature identified by scRNA-seq. (K) Jaccard overlap of the GeoMx spatial profiling data with the PTB scRNA-seq data. (L) Distribution of antimicrobial genes in PTB identified by integrating the GeoMx spatial profiling data with the scRNA-seq data.

# Figure 2

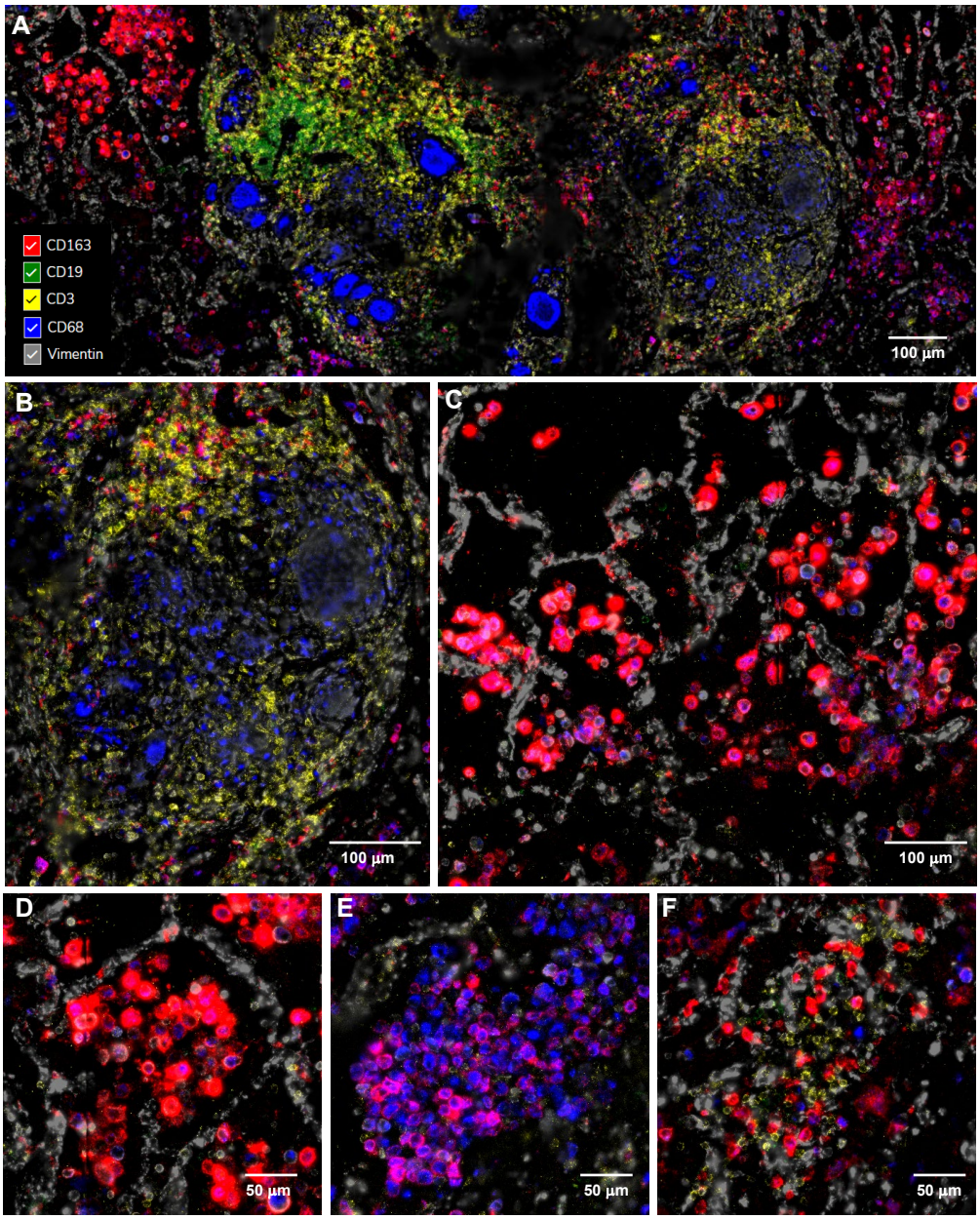


**Figure 2.** Immunofluorescence images obtained using the CosMx spatial profiling with the human protein panel, illustrating the spatial expression of immune cell markers in active pulmonary tuberculosis (TB). (A) Overview of immune cell distribution within the active pulmonary TB lesion. The granuloma core contains CD68+ macrophages (blue) and CD3 T cells (yellow). The granuloma mantle contains CD3 T cells (yellow) and CD19 B cells (green). The alveoli contain prominent CD163 macrophages (red), some with CD68 expression (blue). Vimentin (gray) is present on many cells in the lesions but particularly highlights the alveolar structure by staining alveolar epithelial cells. (B) Localization of immune cells within granulomas. (C-F) Distribution of immune cells in alveolar regions showing heterogeneity of macrophage phenotype and variability in the presence or absence of T cells. Scale bars: 100 µm (low magnification) and 50 µm (high magnification).

# Figure 3

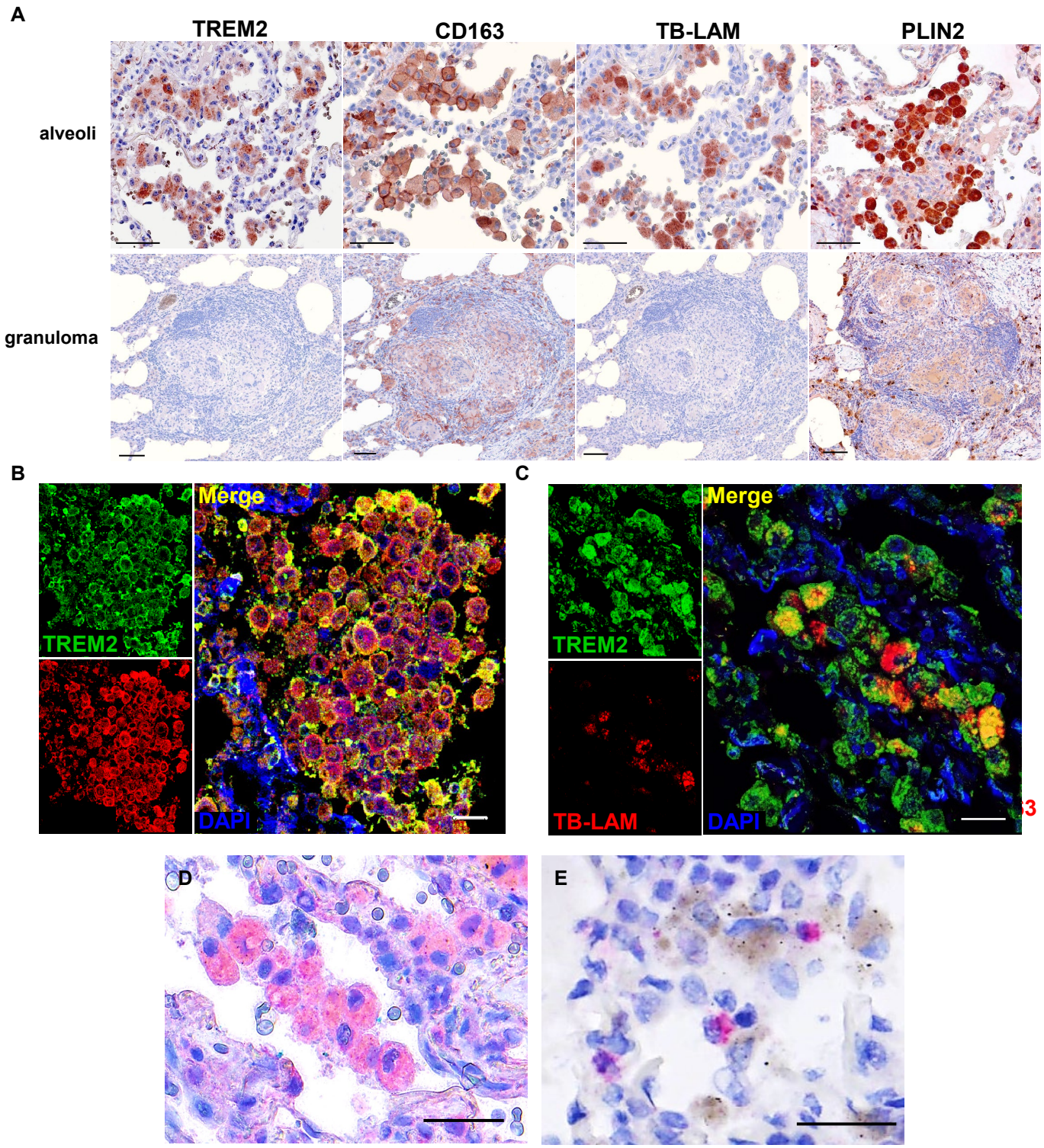


**Figure 3**: Immunohistochemical detection of TREM2+ macrophage signature markers and *M. tuberculosis* lipoarabinomannan (TB-LAM) in pulmonary tuberculosis (TB). (A) TREM2 macrophage signature markers are predominantly detected in the alveolar regions rather than in the granuloma core. (B) TREM2 co-expression with CD163. (C) TB-LAM colocalizes in TREM2+ macrophages. (D) TB-protein detection by immunohistochemistry is observed within foamy macrophages. (E) A similar distribution is observed with Mtb RNA puncta, detected using RNAscope, showing the presence of Mtb in the foamy macrophages. The data is representative of 4 PTB samples. Scale bars: (A)40 µm and (B-E) 20 µm.

# Figure 4

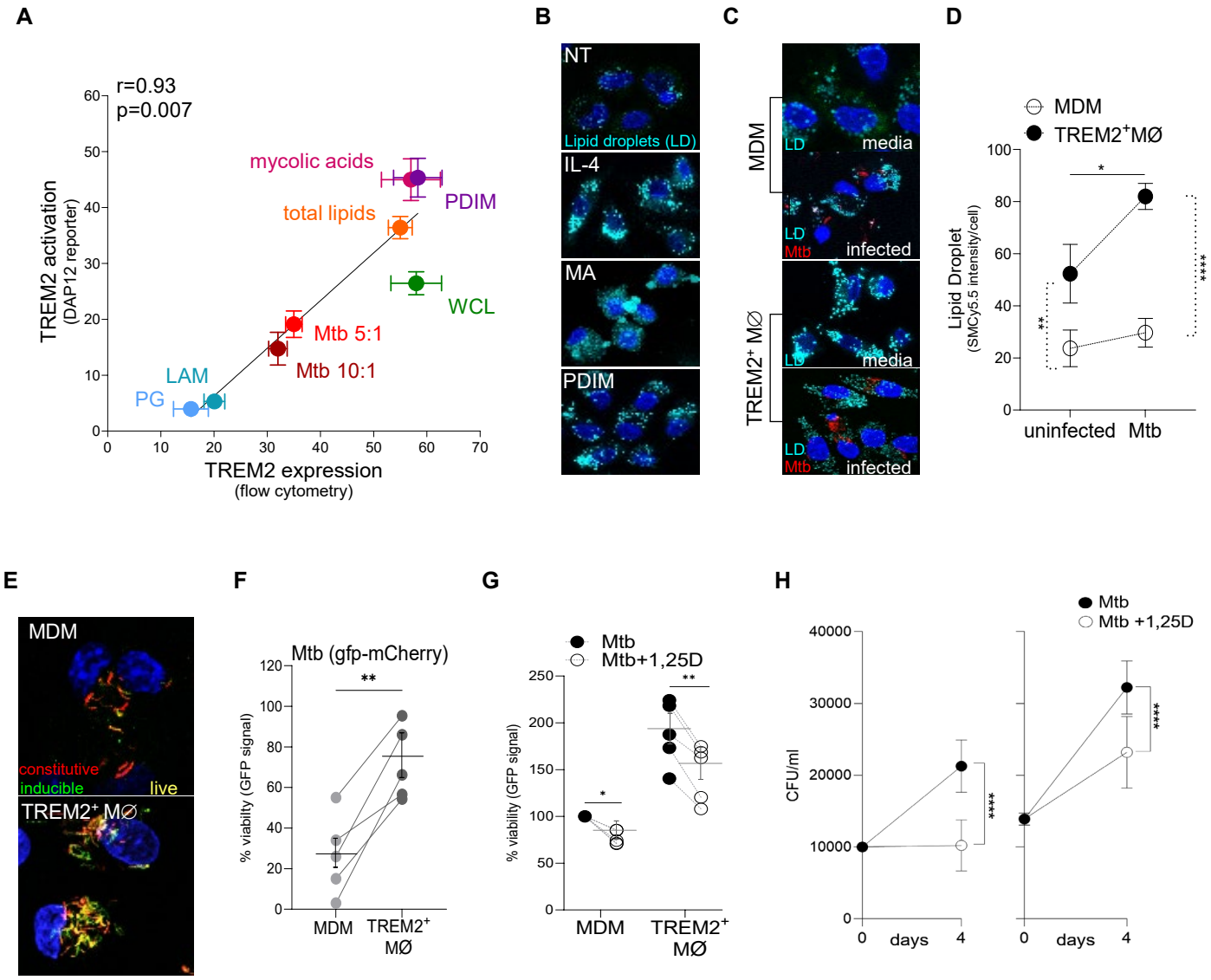


**Figure 4.** TREM2+ macrophage (M∅) interactions with *M. tuberculosis* (Mtb). (A) TREM2 activation correlates with its upregulation in monocyte-derived macrophages (MDMs) stimulated with Mtb-associated ligands (n = 7). (B) Mycolic acids (MA) and phthiocerol dimycocerosates (PDIM) induce lipid droplet (LD) aggregation at levels comparable to IL-4-polarized TREM2+ M∅. (C-D) TREM2+ M∅ exhibit a higher accumulation of lipid droplets than MDMs in uninfected and Mtb-infected conditions (n = 5). Lipid droplets (LD) were labeled with SMCy5.5 (cyan). (E-F) Mtb preferentially proliferates in TREM2+ M∅ compared to MDMs. M∅ were infected with Mtb (GFP-mCherry), with inducible GFP and constitutive mCherry expression (n = 5). (G) M∅ were stimulated with 1,25(OH)2D3 and infected with Mtb (GFP-mCherry) (n = 5). Images were acquired using confocal microscopy, with DAPI used to stain nuclei. Images were acquired using confocal microscopy, with DAPI used to stain nuclei. Quantification was performed using ImageJ. (H) Antimicrobial activity of MDM and TREM2 M∅ following 1,25(OH)2D3 stimulation. Cells were stimulated with 1,25(OH)2D3 and infected with Mtb. The number of viable *M. tuberculosis* bacteria was assessed by CFU assay (n=5). (A, D and F) One-way ANOVA with Tukey multi-comparison test, (G-H) Two-way ANOVA with Fisher multi-comparison test. (B, C, and E) Fluorescent images are representative of 5 individual donors. Statistical significance: * $p \leq 0.05$, ** $p \leq 0.01$, ***$p \leq 0.001$, ****$p \leq 0.0001$.